Application of a Constitutive Model for Swelling Rock to Tunnelling

B. Schädlich[1], T. Marcher[2] and H.F. Schweiger[1]
[1]Institute for Soil Mechanics and Foundation Engineering, Graz University of Technology, Graz, Austria
[2]ILF Consulting Engineers, Innsbruck, Austria
E-mail: bert.schaedlich@tugraz.at

ABSTRACT: Swelling due to chemical processes is a well-known problem in tunnelling in anhydritic rocks and certain types of claystone. If the swelling rock mass is exposed to water due to tunnel excavation or natural water influx, in anhydritic rocks large deformations of more than 1 m can be observed, which are typically concentrated at the tunnel invert. Estimating swelling deformations and swelling pressures is of paramount importance for the design of durable underground structures in such materials. This paper presents the results of a numerical back analysis of measured swelling deformations with a simple constitutive model, using swelling parameters derived from laboratory swelling tests.

1.   INTRODUCTION

Starting more than 130 years ago with the construction of the Schanz railway tunnel in southern Germany, swelling phenomena have caused major difficulties in many tunnelling projects. When water is allowed to infiltrate the swelling rock mass, chemical processes within the rock matrix are initiated which can result in large volume increase. As water aggregates at the tunnel invert, typically large invert heave deformations evolve if no or a rather flexible invert lining is installed. In the case of a rigid support concept, large swelling pressures develop at the tunnel lining.

The most prominent rock types exhibiting swelling behaviour are certain types of claystone and anhydrite-bearing rocks. Even though their macroscopic swelling behaviour may appear similar, the underlying chemical processes are fundamentally different. In both cases, however, swelling depends not only on material characteristics but also on the availability of water.

Although a great amount of practical experience has been gained in the last decades, tunnelling in swelling rock is still a very challenging task, as the recent examples of the Engelbergtunnel in southern Germany and the Chienbergtunnel in Switzerland demonstrate. Reliable prediction of swelling pressures and swelling deformations especially in anhydritic rock is extremely difficult due to the heterogeneity of the material and the complexity of the involved transport mechanisms (Anagnostou et al. 2010).

This paper presents a back analysis of in-situ measurements of the Pfaendertunnel (Austria) in swelling claystone. It is demonstrated that calculated swelling deformations are very sensitive to the choice of swelling parameters, in particular to the maximum swelling stress. As laboratory tests typically deliver a wide range of swelling parameters, this may to some extent explain the large variation of measured swell heave deformations in apparently homogenous tunnel sections.

All stresses and strains are taken to be tension positive.

2.   SWELLING PROCESSES

2.1   Clay swelling

Swelling of clays comprises two different mechanisms: Innercrystalline swelling and osmotic swelling.

Innercrystalline swelling is related to the incorporation of water within the clay particles and requires a very large pressure (up to -400 MPa in the case of Montmorillonite) to be suppressed. As such high pressures are usually not provided by the natural environment, innercrystalline swelling has already taken place in most natural clays and does not contribute to swelling deformations after tunnel excavation.

The more relevant swelling mechanism from a practical point of view is osmotic swelling, which is caused by differences in cation concentration in the clay matrix and in the free pore water (Figure 1). After innercrystalline swelling has taken place, sodium cations (surrounded by water molecules) tend to align at the surface

of the clay particles. A electric double layer is formed, which consists of the negatively charged aluminosilicate layers at the centre and a positively charged, diffuse cation cloud at the surface. Water is drawn in between the clay particles as a result of the difference in cation concentration with respect to the free pore water.
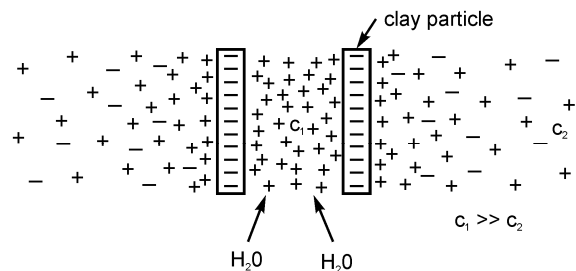

Figure 1 Osmotic swelling of clay minerals (after Madsen & Müller-Vonmoss 1989)

Swelling deformations decrease with the logarithm of the applied stress (Figure 2), which is known as Grob's swelling law (Grob 1972). Consequently, allowing for a small amount of deformation already reduces the swelling pressure significantly, which is an important aspect for the design of underground structures.
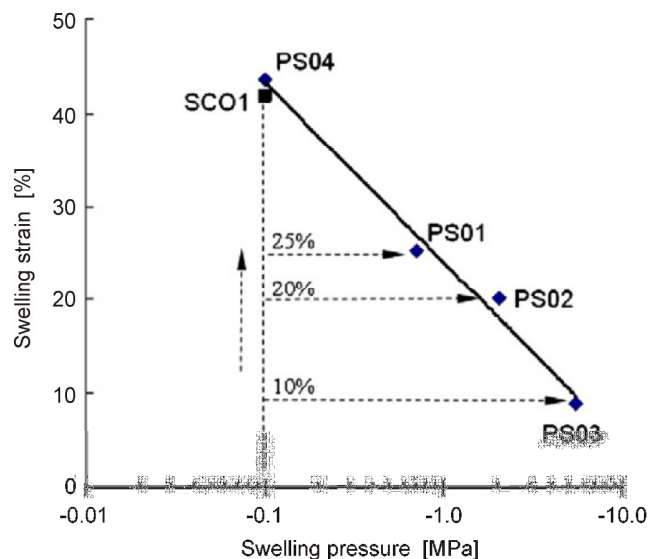

Figure 2 Swelling test results of bentonite-claystone mixtures (after Wang et al. 2012)

2.2 Anhydrite swelling

Swelling of rock containing anhydrite like the gypsum keuper formation in south-western Germany is the result of the chemical reaction of unleached anhydrite ($CaSO_4$) with water to gypsum ($CaSO_4 \cdot H_2O$), Eq. 1. The specific volume of gypsum is about 60% higher than that of the unleached anhydrite.

$$Ca^{2+} + SO_4^{2-} + 2H_2O \rightarrow CaSO_4 \cdot 2H_2O \tag{1}$$
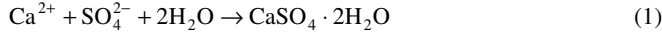
The gypsum is initially dissolved in the pore water and only starts to precipitate once the gypsum saturation concentration is exceeded. The growth of gypsum crystals in cracks and macropores further contributes to the volume increase resulting from the chemical reaction itself. Due to the high solubility of gypsum, swelling can occur in parts of the rock mass which are different from the area where the anhydrite was initially dissolved.

The applicability of Grob's swelling law to anhydrite is highly debated. Due to the slow evolution of swelling deformations in anhydritic rock, there are no experimental results available for final swelling deformation and swelling pressures (Anagnostou et al. 2010). Extrapolation of laboratory test results seems to indicate, that swelling deformations remain high and almost constant up to a stress level of ~-4.0 MPa with a sharp subsequent drop to almost zero (Pimentel 2007). This is in contrast to field observations in the Freudenstein test gallery, where invert heave was significantly reduced by increasing the support pressure with prestressed anchors, even though no final swelling state has been reached yet. Most constitutive models for swelling rock employ Grob's swelling law also for anhydritic rock (Wittke & Wittke 2005).

3. SWELLING ROCK MODEL

The constitutive model used in this paper is based on Wittke-Gattermann (1998) and was implemented by T. Benz (Benz 2012) as a user-defined soil model for the finite element software PLAXIS. The main features of the model are briefly explained in the following section.

3.1 Stress dependency of swelling

The relationship between final swelling strains $\varepsilon_i^{q(t=\infty)}$ and the axial stress in the axial direction i (i = 1, 2, 3) is given by Grob's semi-logarithmic swelling law (Figure 3).

$$\varepsilon_i^{q(t=\infty)} = -k_{qi} \cdot \log_{10}\left(\frac{\sigma_i}{-\sigma_{q0i}}\right) \tag{2}$$

k_{qi} is the (axial) swelling parameter, σ_i is the axial stress and σ_{q0i} is the maximum swelling stress in the axial direction i. The swelling curve is limited at -10 kPa to avoid excessive swelling strains at low or tensile stresses. Swelling strains are calculated in the coordinate system of principle stresses without any interaction of swelling in the different directions.
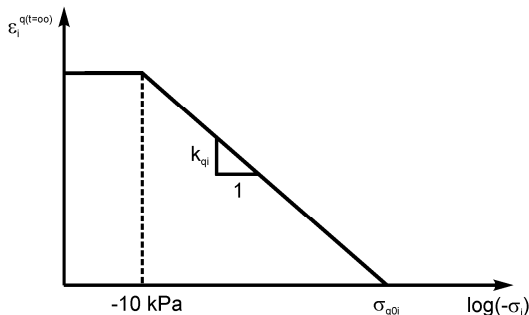

Figure 3 Semi-logarithmic swelling law (Grob 1972)

3.2 Evolution of swelling with time

The model is based on exponential decay of the difference between the current swelling strain and the final swelling strain (Kiehl 1990). The swelling rate is determined by the parameter η_q, which gives the time to reach the final swelling strain based on the initial inclination of the time swelling curve (Figure 4).

$$\varepsilon_i^{q(t)} = \varepsilon_i^{q(t=\infty)} \cdot \left(1 - e^{-t/\eta_q}\right) \tag{3}$$

$$\dot{\varepsilon}_i^{q(t)} = \frac{\left(\varepsilon_i^{q(t=\infty)} - \varepsilon_i^{q(t)}\right)}{\eta_q} \tag{4}$$

In incremental form, the swelling strain increment in the current time step is calculated from the information provided at the beginning of the step:

$$\varepsilon_i^{q(t+\Delta t)} = \varepsilon_i^{q(t)} + \frac{\left(\varepsilon_i^{q(t=\infty)} - \varepsilon_i^{q(t)}\right)}{\eta_q} \cdot \Delta t \tag{5}$$
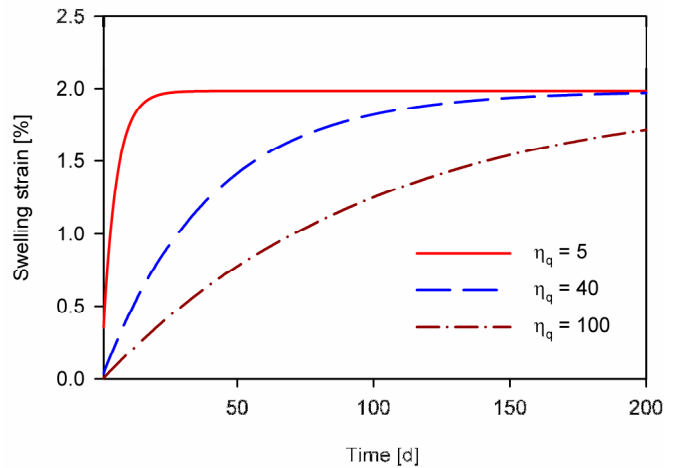

Figure 4 Influence of η_q on evolution of swelling strains

The influence of elastic and plastic volumetric strains, ε_v^{el} and ε_v^{pl}, can be taken into account by the parameters A_{el} and A_{pl}:

$$\eta_q = 1/\left(A_0 + A_{el} \cdot \varepsilon_v^{el} + A_{pl} \cdot \varepsilon_v^{pl}\right) \tag{6}$$

Positive volumetric strains (loosening of the material) result in faster approach of the final swelling strain, while negative volumetric strains delay or may even stop the evolution of the swelling strains. A_0 is a threshold value, resulting in a constant value of η_q. This approach accounts for the dependency of the swelling rate on the penetration rate of water, which changes with the permeability of the rock mass and the thickness of the swelling rock layer. Due to their dependency on the thickness of the swelling rock layer, A_0, A_{el} and A_{pl} usually cannot be derived from laboratory swelling tests.

3.3 Plastic strains

Plastic strains are calculated according to a Mohr-Coulomb failure criterion with tension cut-off. Shear strength is defined by effective friction angle, φ', and effective cohesion, c'. The direction of the plastic strain increment is defined by a non-associated flow rule, using the angle of dilatancy, ψ. The elastic ($\Delta\varepsilon^{el}$), plastic ($\Delta\varepsilon^{pl}$) and swelling strain increment $\Delta\varepsilon^q$ add up to the total strain increment $\Delta\varepsilon$:

$$\Delta\boldsymbol{\varepsilon} = \Delta\boldsymbol{\varepsilon}^{el} + \Delta\boldsymbol{\varepsilon}^{pl} + \Delta\boldsymbol{\varepsilon}^q \tag{7}$$

Within a finite element calculation scheme, an iterative procedure on stress point level is required to find the stress state which satisfies the constitutive equations for the given total strain increment. The model employs an approach proposed by Heidkamp & Katz (2002), which is based on an implicit backward-Euler-scheme with integrated line search.

4. PFAENDERTUNNEL CASE STUDY

4.1 Project description and geological overview

The 6.7km long first tube of the Pfaendertunnel near Bregenz (Austria) was constructed in 1976-1980 according to the principles of the New Austrian Tunnelling method (NATM). While top heading and bench excavation were carried out without major difficulties, significant invert heave of up to 30 cm was observed after about 75% of the tunnel length was excavated. These observations lead to detailed laboratory investigations of the swelling characteristics of the Pfaenderstock material, an extensive monitoring program and to the installation of additional anchors in the tunnel invert.

Figure 5 Pfaendertunnel cross section 1st tube
(after John & Pilser 2011)

The Pfaenderstock consists of various sedimentary molasse rocks (sandstone, conglomerate, claystone, marl), which were deposited in the area north of the Alps between the early Oligocene and the older Pliocene. The rock mass is characterised by significant interstratification, with layers varying in thickness and in general dipping into the longitudinal tunnel direction. The maximum overburden is 350 m. Minor water inflow was observed in the areas close to the tunnel portals, while the central part of the tunnel was essentially dry during excavation.

4.2 Laboratory swelling tests

The marl layers were identified as the rock type contributing the most to the swelling phenomena observed after tunnel excavation. This was attributed to two factors:
1. The marl contains a significant proportion of Montmorillonite clay minerals (up to 30% of the total rock mass), which are especially prone to absorb water and increase in volume.
2. The marl is in particular present in fault zone areas, in which the influx of water into the rock mass is greatly facilitated by existing fissures.

Laboratory swelling tests were conducted at different research institutions, using different testing methods and equipment. Czurda & Ginther (1983) carried out swell heave tests in oedometric conditions, i.e. the evolution of vertical strain was monitored under constant vertical stress. Weiss et al. (1980) used a three-axial device in which the axial swelling pressures could be measured independently. Their tests were based on either allowing no deformation (swell pressure test) or no swelling pressure (free swelling test).

Czurda & Ginther (1983) distinguished between samples of undisturbed molasse marl (series A, Figure 6), retrieved outside the fault zones, and the fault zone material (series B, Figure 7). Series A samples showed higher maximum swelling potential, but lower maximum swelling pressures than the samples of series B. This difference was attributed to relaxation and swelling of the series B samples before the samples could be tested. Due to fissuring and higher water content, evolution of swelling strains may have taken place faster in the series B samples, which resulted in part of the swelling to occur before testing. Consequently, the in situ swelling potential of the series B material may be higher than tested and in the range of the undisturbed series A samples.

It is also worth noting, that Czurda & Ginther (1983) could only apply axial stresses of up to -300 kPa, which were not sufficient to suppress swelling completely. The maximum swelling pressures were therefore extrapolated from tests at lower stress levels, assuming the validity of Grob's swelling law. As this procedure lead to very high maximum swelling pressures for the series B samples, Czurda & Ginther (1983) speculated that the $\varepsilon_q - \sigma_{vert}$ - curve may show a kink at higher stresses, resulting in maximum swelling stresses similar to the series A samples.

Figure 6 Swelling test results, series A after Czurda & Ginther (1983)

Figure 7 Swelling test results, series B after Czurda & Ginther (1983)

Weiss et al. (1980) obtained a much wider range of experimental results (Figure 8), in some cases with samples from the same borehole. They did not distinguish between samples retrieved inside and outside the fault zone area. The upper boundary of their test results roughly coincides with the mean of the series A samples reported by Czurda & Ginther (1983). The samples with significant swelling also exhibited approximately isotropic behaviour, i.e. both the maximum swelling stresses and the swelling potentials were almost independent of sample orientation. Results shown in Figure 8 are mean values, averaged over the three axial directions. Weiss et al. (1980) also analysed the mineral content of the samples and found a strong correlation of maximum swelling stress and Montmorillonite content.

For the back analysis of the field measurements two swelling parameter sets are considered, which represent the upper and lower boundary of the test results of Czurda & Ginther (1983). The time swelling parameters A_0, A_{el} and A_{pl} were calibrated to match the in situ time-swelling curve.
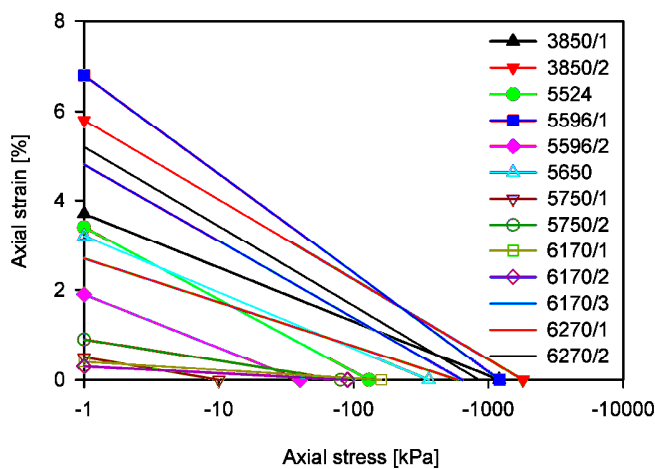
Figure 8 Swelling test results after Weiss et al. (1980)

4.3 Numerical model and material parameters

The numerical model used in this study is shown in Figure 9, with basic material parameters for the different layers given in Table 1. The model is discretised with 15-noded triangular finite elements. Tunnel geometry and basic material parameters of the marl layer at tunnel height have been taken from John et al. (2009). Soil weight is uniform with $\gamma = 24$ kN/m³, and a tensile strength of 0.1·cohesion has been assumed. Soil layers of 10 m and 25 m thickness have been placed at the surface to avoid unrealistic stiffness close to the ground surface. Tunnel overburden is ~200 m above the tunnel crown, which is representative of the cross section at km 5+373.

Linear elastic plate elements are used for the temporary shotcrete lining, with $E = 7.5$ GPa for the young and $E = 15$ GPa for the cured shotcrete. Shotcrete lining thickness is 20 cm in the top heading and 10 cm at the invert. The final concrete lining is modelled with volume elements assuming linear elastic behaviour and a stiffness of $E = 30$ GPa. The final lining thickness varies between 50 cm at the invert and 25 cm at the crown.

Swelling is confined in the model to an area of 15 m x 15 m below the tunnel invert. As water is required to start the swelling process, and water due to drilling blastholes and natural water inflow accumulates at the tunnel invert, observations show that swelling in practice only affects the tunnel invert (Berdugo et al. 2009). The potential swelling zone in the numerical model is deep enough to allow the full development of swelling deformations below the tunnel invert.

Swelling parameters for the different parameter sets are listed in Table 2. Sets 1a and 1b have a higher swelling potential k_q, but a lower maximum swelling stress than sets 2a and 2b. The maximum swelling stress of set 2a and 2b is ~80% of the initial vertical stress

at tunnel level and represents the lower edge of the experiments of Czurda & Ginther (1983) for the fault zone material. Sets 1a, 1b and 2a only employ A_0 for the time dependency of swelling, while in set 2b evolution of swelling with time is entirely governed by elastic volumetric strains.
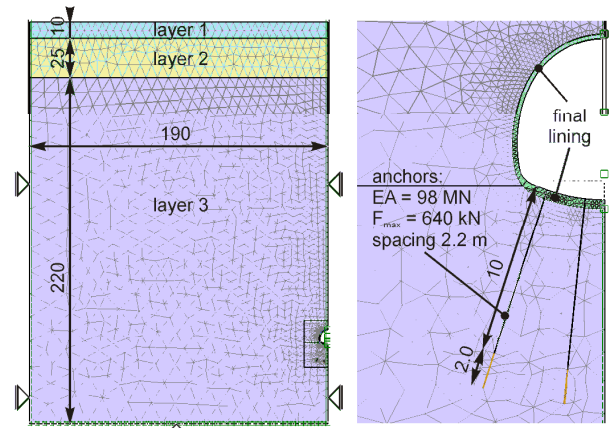

Figure 9 Finite element model (dimensions in m)

Table 1 Basic material parameters

Parameter	Layer 1	Layer 2	Layer 3
Young's modulus E'	50 MPa	250 MPa	2500 MPa
Poisson's ratio v'	0.35	0.35	0.35
Friction angle φ'	34°	34°	34°
Cohesion c'	10 kPa	100 kPa	1000 kPa

Table 2 Swelling parameters

Parameter	Set 1a	Set 1b	Set 2a	Set 2b
Swelling potential k_q [%]	3.0	3.0	0.75	0.75
Max. swelling stress σ_{q0} [kPa]	1000	1500	4000	4000
A_0	5.0e-3	2.5e-3	3.0e-3	0.0
A_{el}	0.0	0.0	0.0	9.0
A_{pl}	0.0	0.0	0.0	0.0

4.4 Calculation phases

The calculation phases aim to model the construction process as reported by John (1982). After top heading / invert excavation (assuming stress pre-relaxation factors of 75% and 37.5%, respectively), the concrete invert arch is installed. After a swelling phase of 65 days, the final lining is activated, followed by another swelling phase of 115 days. John reported that the decision on invert anchoring and pre-stressing was based on the swell heave deformations observed up to this point. In the cross section considered here this resulted in applying a pattern with 2.2m anchor spacing.

The calculation phases are performed in the following order:
1. Initial stresses ($K_0 = 0.8$)
2. Pilot tunnel excavation wished-in-place
3. 75% stress pre-relaxation of top heading
4. Top heading excavation and shotcrete installation (shotcrete young)
5. 37.5% stress pre-relaxation of invert, top heading shotcrete switched to cured
6. Invert excavation and shotcrete installation (shotcrete young)
7. Invert arch installation
8. 65 days of swelling
9. Installation of final lining (ring closure)
10. 115 days of swelling
11. Anchor prestressing (0.8x640 kN = 512 kN per anchor)
12. 7000 days of swelling

4.5 Results

4.5.1 Evolution of invert heaves with time

Figure 11 compares the time-swelling curves calculated with the different parameter sets with the measured invert heave in km 5+373. The measurements plot close to a straight line in logarithmic time scale, which cannot be reproduced exactly by the exponential approach employed in the model. The match with the measured invert heave is, however, sufficient from a practical point of view.

Set 1a delivers too little invert heave (10 mm), and the development of deformations completely stops after activating the prestressed anchors. Increasing the maximum swelling stress by 50% (set 1b) yields ~50% more deformation and a better match with the measurements. While such a significant influence may be expected, it should be noted that experimental results for these two sets plot so close to each other that either of the two parameter sets appears justified (Figure 6).

Surprisingly, sets 2a and 2b – which represent much smaller free-swell deformations – deliver more invert heave than sets 1a and 1b. This is a result of the higher maximum swelling stress assumed in sets 2a and 2b, which activates swelling in deeper rock layers, yet with a small swelling potential. Swelling deformations are thus more widely distributed with set 2a and 2b than they are with sets 1a and 1b.

Modelling the evolution of swelling with time entirely in dependence on elastic volumetric strains (set 2b) results in a slightly more prolonged time-swell-curve than using a constant value of A_0 (set 2a). In set 2b the rate of swelling does not only decrease due to the convergence with the final swelling strain, but also due to negative elastic volumetric strains. The large positive volumetric strains after tunnel excavation are gradually reduced in the swelling phases by the increasing swelling pressure.
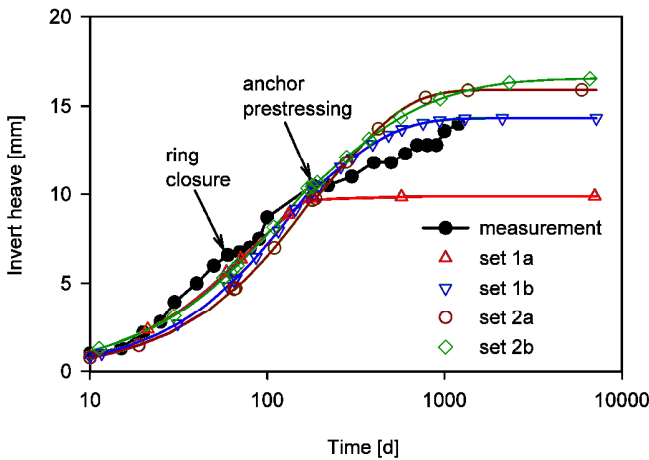
Figure 10 Development of invert heave with time

4.5.2 Swelling pressure

Figure 11 shows the distribution of swelling pressure on the tunnel invert lining for different stages in time for parameter set 1b. The circumferential distance L is measured from the tunnel invert, such that $L = 0$ m is directly at the invert and $L = 5$ m is the end of the swelling area.

Due to the stiffer support provided to the tunnel lining at the sides of the tunnel, the maximum swelling pressure does not occur at the tunnel invert but at a distance of ~3.8 m.

Anchor prestressing increases the normal stress on the lining by about 90 kPa. The difference to the distributed prestressing force of $(0.8*640kN / 2.2m / 2.2m) = 106kN/m^2$ is a result of the already closed final lining, which distributes part of the applied load in circumferential direction. Comparing the increase in pressure to the swelling line of set 1b at -200 to -300 kPa (Figure 6) explains the limited influence of prestressing in the numerical calculations. Even

though anchor prestressing increases the pressure by ~45%, reduction of final swelling strain is only about 18% due to the semi-logarithmic swelling law. Additionally, the effect of prestressing diminishes rapidly with increasing distance to the tunnel, and the deeper rock layers remain virtually unaffected.
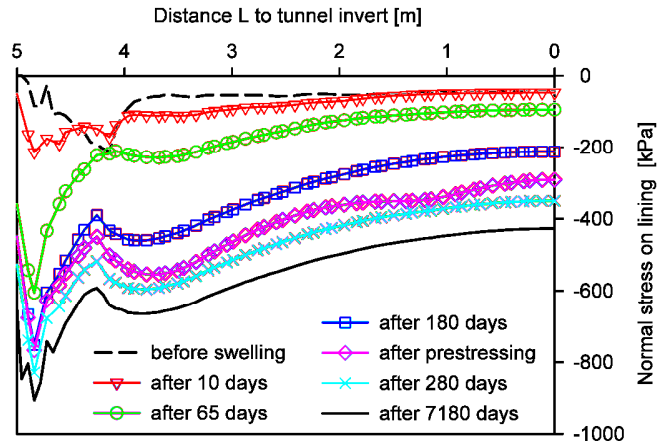

Figure 11 Development of pressure on the lining (set 1b)

4.5.3 Distribution of swelling strains over depth

The proportion of the rock mass which is affected by swelling depends primarily on the maximum swelling stress. For set 1b (σ_{q0} = 1500kPa) the swelling zone is confined to about 2m below the tunnel invert, which matches well with the sliding micrometer measurements in cross section km 5+820 (Figure 12). The swelling zone with set 2b (σ_{q0} = 4000 kPa) is much deeper due to the higher maximum swelling pressure, even though similar invert heave is obtained with both parameter sets. These results indicate that σ_{q0} is rather in the range of 1000-2000 kPa than close to the in-situ stresses.

It should be noted, that the magnitude of swelling differs considerably between cross sections km 5+373 and km 5+820. This is presumably a result of a lower swelling potential in km 5+820, as final invert heave 10 years after construction amounted to only 5mm in this section (John et al. 2009), compared with ~14mm in 3 years in km 5+373.
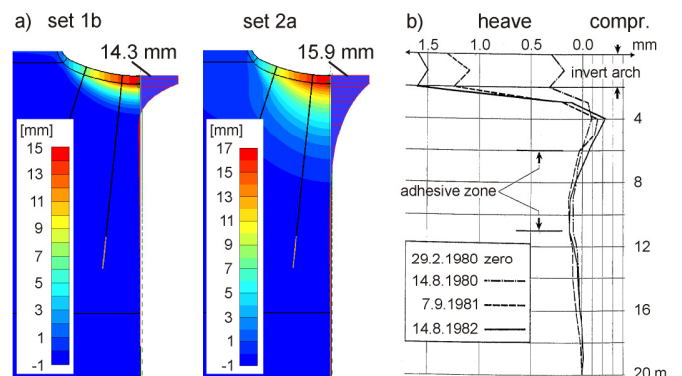

Figure 12 Profile of vertical displacements, a) numerical analysis at t = 7180 d, b) measurements km 5+820 (after John 1982)

4.6 Parameter variations

4.6.1 Variation of maximum swelling pressure σ_{q0}

The results presented in section 4.5 showed that invert heave is notably sensitive to the maximum swelling pressure σ_{q0} assumed in the numerical analysis. As the variation of this parameter is rather large in the laboratory swelling tests – albeit concealed by the logarithmic stress scale – σ_{q0} has been varied from 500kPa to 2000kPa. Other parameters have been taken from set 1b (k_q = 3%).

Results indicate a linear increase of invert heave with σ_{q0} (Figure 13). The swelling zone below the tunnel invert grows almost linearly with σ_{q0}, while the shape of the displacement profile remains the same (Figure 14). The larger invert heave is therefore a result of the increasing depth of the swelling zone, which expands as areas with higher stress levels prior to swelling get activated if larger values of σ_{q0} are employed.
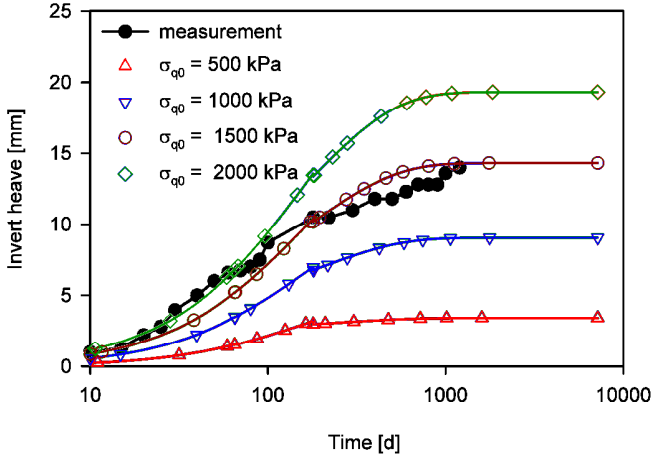

Figure 13 Evolution of invert heave with time for different maximum swelling stresses σ_{q0}
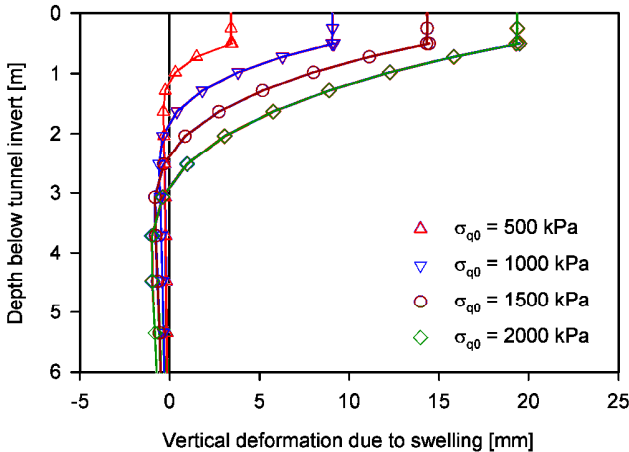
Figure 14 Vertical displacement profiles below tunnel invert for different maximum swelling stresses σ_{q0}

4.6.2 Variation of swelling potential k_q

The invert heave at the tunnel lining is also influenced by the swelling potential k_q. This parameter was varied from 1% to 4%, while employing a constant maximum swelling stress of $\sigma_{q0} = 1500$ kPa (with other parameters taken from set 1b). Similar to increasing σ_{q0}, invert heave deformations rise with increasing values of k_q (Figure 15). However, the depth up to which swelling occurs is not influenced by changes of k_q (Figure 16). The larger invert heave for larger values of k_q is clearly a result of higher swelling strains directly underneath the tunnel invert and not due to changes in the size of the swelling zone.

4.6.3 Variation of time swelling parameters

The swelling parameters A_0 and A_{el} were calibrated at the measured time-swelling curve. As may be expected, development of invert heave with time is very sensitive to the chosen value of A_0 (Figure 17), with a faster evolution of swelling deformations for a larger value of A_0. Final swelling deformations, however, are only modestly influenced by the choice of A_0, as the impact of the final lining completion and the pre-stressed anchors is small.
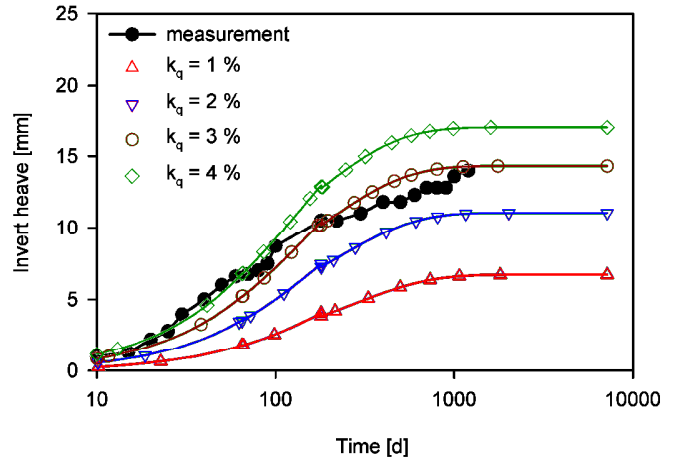

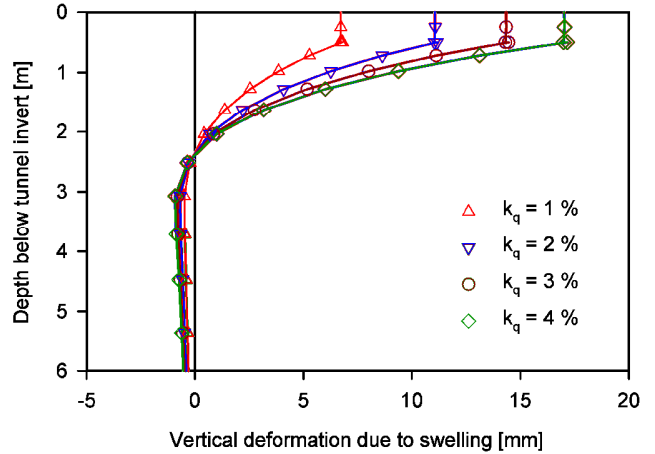Figure 15 Evolution of invert heave with time for different swelling potentials k_q

Figure 16 Vertical displacement profiles below tunnel invert for different swelling potentials k_q
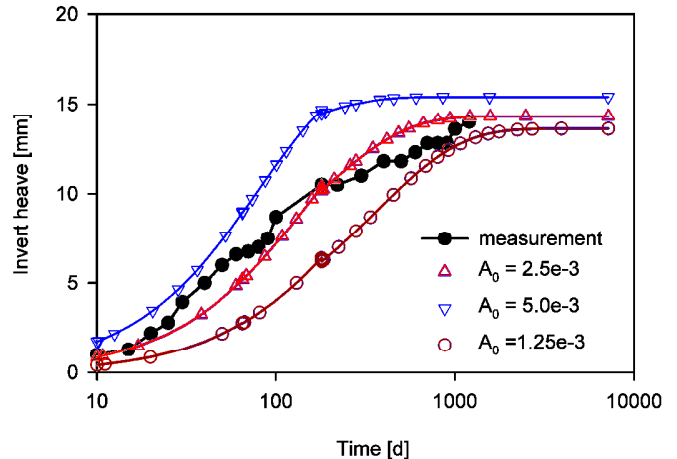

Figure 17 Variation of time swelling parameters (set 1b)

4.6.4 Variation of rock stiffness

In most practical cases, the stiffness of the rock mass is an experience-based estimate rather than a parameter which is thoroughly derived from laboratory or in situ tests. Even if such tests are available, the heterogeneity of the rock mass usually results in some variability of testing results. In the constitutive swelling model the rock stiffness can influence swelling deformations in multiple ways:

1. The lower the rock stiffness, the less stresses are transferred by the swelling rock mass on the tunnel lining, as swelling strains can be compensated by elastic strains with less increase in stresses. Consequently, swelling deformations will be smaller.
2. The lower the elastic stiffness, the less bedding is provided to the tunnel by the rock at the bench and crown. Consequently, invert heave will increase with lower rock stiffness.
3. If $A_{el} \neq 0$, evolution of swelling deformations with time depends on elastic strains. Starting after tunnel excavation, lower elastic stiffness accelerates the development of swelling strains, as the initial elastic volumetric strains are larger.

The sensitivity of swelling with regard to rock stiffness was studied by varying the Young's modulus of layer 3 by a factor of 2 and 0.5 with swelling parameter set 1b. The parameters of the two layers at the surface were kept constant.

Increasing the rock stiffness resulted in a slight reduction of final swelling deformation and a marked increase of swelling pressure at the tunnel invert (Figure 18). In the present case study, the stiffer bedding at the tunnel crown obviously has more influence than the higher swelling pressure at the tunnel invert. The overall influence of rock stiffness on swelling deformations is small.
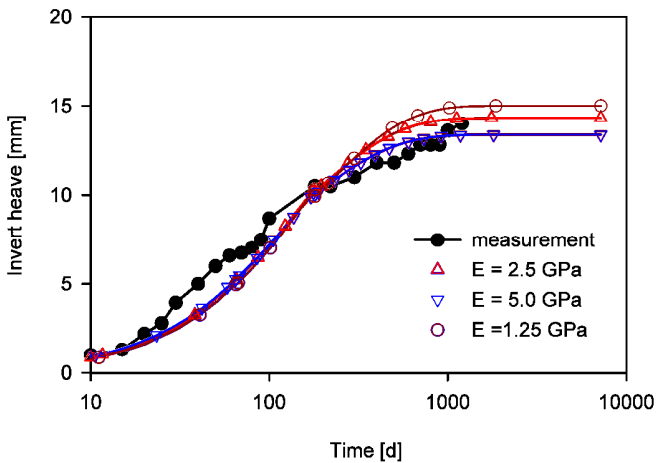

Figure 18 Variation of rock stiffness (set 1b)

4.6.5 Variation of stress pre-relaxation factors

The pre-relaxation factors for top heading and invert excavation account for 3D-stress redistribution ahead of the tunnel face, which naturally cannot be modelled directly in 2D plane strain calculations. These factors are usually an empirical estimate rather than being systematically derived from 3D calculations or in-situ measurements. As stress pre-relaxation influences the stress state and deformations after tunnel excavation, it may be expected that the choice of these factors has some effect on swelling deformations.

Assuming pre-relaxation factors of 50% / 25% (top heading/invert excavation), however, delivers virtually identical time-swell curves as with 75% / 37.5% (Figure 19). The limited influence of stress pre-relaxation on final swelling deformations can be explained by the two-step excavation process. No temporary invert lining is installed after top heading excavation, and hence there is an almost complete stress relaxation in the area of the final tunnel invert, regardless of the choice of pre-relaxation factors.

Additionally, the stiffness of the rock mass (2.5GPa) is rather high compared to the shotcrete lining (7.5GPa), which means that the influence of lining installation and pre-relaxation factors on rock mass deformation is small.
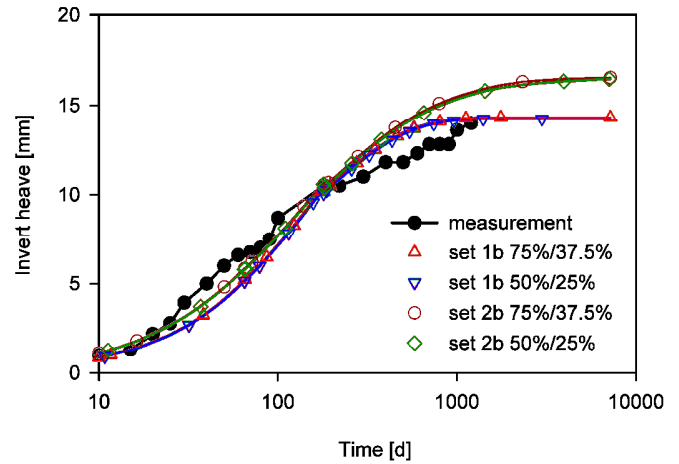

Figure 19 Variation of stress pre-relaxation

5. CONCLUSIONS

This paper presented the results of a back analysis of measured swelling deformations in the Pfaendertunnel (Austria). A constitutive model based on Grob's swelling law and exponential convergence with final swelling strains over time was used for the numerical calculations. Input swelling parameters were derived from swell heave tests published by Czurda & Ginther (1983). The following conclusions can be drawn from this study:

1. The constitutive swelling model used in this study is in principle capable of reproducing the swelling behaviour of claystone as observed in tunnel excavations. Different sets of swelling potential k_q and maximum swelling stress σ_{q0} may deliver very similar swelling deformations at the tunnel lining, as increasing σ_{q0} is roughly equivalent to increasing k_q.
2. The size of the swelling zone below the tunnel invert depends primarily on the maximum swelling stress σ_{q0}. Good match with the measured displacement profile was obtained with σ_{q0} = 1500kPa, which represents the upper edge of the experimental results on undisturbed molasse marl. Using σ_{q0} close to the initial vertical stress of 4900kPa delivered a too large swelling zone.
3. The invert heave measurements plot close to a straight line in logarithmic time scale, which cannot be exactly reproduced by the exponential approach used in the constitutive model. The match with the measured evolution of swelling, however, is sufficient from a practical point of view.
4. Calculated invert heave is in particular sensitive to the choice of the maximum swelling stress σ_{q0}. While the impact of changes of σ_{q0} at a single stress point is limited due to the semi-logarithmic swelling law, the size if the swelling zone in the numerical model changes almost linearly with σ_{q0}, which consequently results in a roughly linear relation between invert heave and σ_{q0}.

6. REFERENCES

Anagnostou, G., Pimentel, E., and Serafeimidis, K. (2010) "Swelling of sulphatic claystones – some fundamental questions and their practical relevance", Geomechanics and Tunnelling, 3 (5), pp. 567-572.

Benz, T. (2012) Personal communication.

Berdugo, I. R., Alonso, E., Romero, E. and Gens, A. (2009). "Tunnelling and Swelling in Triassic Sulphate–Bearing Rocks. Part I. Case studies from Baden–Württemberg", Revista Epsilon 12, 1–17.

Czurda, K. A., and Ginther, G. (1983) "Quellverhalten der Molassemergel im Pfänderstock bei Bregenz, Österreich", Mitt. österr. geolog. Ges., 76, pp. 141-160.

Grob, H. (1972) "Schwelldruck im Belchentunnel", Proc. Int. Symp. für Untertagebau, Luzern, pp. 99-119.

Heidkamp, H., and Katz, C. (2002). „Soils with swelling potential - Proposal of a final state formulation within an implicit integration scheme and illustrative FE-calculations", Proc. of the 5th World Congress on Comp. Mec., Vienna, Austria.

John, M. (1982) "Anwendung der neuen österreichischen Tunnelbauweise bei quellendem Gebirge im Pfändertunnel" Proc. of the 31st Geomechanik Kolloquium, Salzburg, Austria.

John, M., Marcher, T., Pilser, G., and Alber, O. (2009) "Considerations of swelling for the 2nd bore of the Pfändertunnel", Proc. of the World Tunnel Congress 2009, Budapest, Hungary, pp. 50-61.

John, M., and Pilser, G. (2011) "Criteria for selecting a tunnelling method using the first and the second tube of the Pfänder tunnel as example", Geomechanics and Tunnelling, 4(11), pp. 527-533.

Kiehl, J. R., (1990) „Ein dreidimensionales Quellgesetz und seine Anwendung auf den Felshohlraumbau", Proc. 9. Nat. Rock Mech. Symp., Aachen 1990, pp. 185 - 207.

Madsen, F. T., and Müller-Vonmoss, M. (1989) "The swelling behaviour of clay", Applied Clay Science 4, pp. 143-156.

Pimentel, E. (2007), "Quellverhalten von Gesteinen – Erkenntnisse aus Laboruntersuchungen", Mitteilungen der Schweizerischen Gesellschaft für Boden- und Felsmechanik, Heft 154, Fribourg, pp. 13–20.

Wang, Q., Tang, A. M., Cui, Y. J, Delage, P., and Gatmiri, B. (2012) "Experimental study on the swelling behaviour of bentonite/claystone mixture", Engineering Geology, 124, pp. 59-66.

Weiss, E. H., Müller, H. M., Riedmüller, G., and Schwaighofer, B. (1980) "Zum Problem quellfähiger Gesteine im Tunnelbau", Geolog. Paläont. Mitt. Innsbruck, 10(5), pp. 207-210.

Wittke-Gattermann, P. (1998) "Verfahren zur Berechnung von Tunnels in quellfähigem Gebirge und Kalibrierung an einem Versuchsbauwerk", Geotechnik in Forschung und Praxis, WBI-PRINT 1, Verlag Glückauf, Essen.

Wittke, W., and Wittke, M. (2005) "Design, construction and supervision of tunnels in swelling rock", Proc. 31st ITA World Tunnelling Congress 2005, pp. 1173-1178.